Breast Tomosynthesis: Aspects on detection and perception of simulated lesions

Timberg, Pontus

2011

Breast Tomosynthesis

Aspects on detection and perception of simulated lesions

Pontus Anders Sigurd Timberg

Medical Radiation Physics
Department of Clinical Sciences, Malmö
Faculty of Medicine, Lund University
Skåne University Hospital
2011

LUND
UNIVERSITY

Cover: Piece of art for individual interpretation.

Thesis for the Degree of Doctor of Medicine
Lund University
Faculty of Medicine Doctoral Dissertation Series 2011:81
Medical Radiation Physics
Department of Clinical Sciences, Malmö
Skåne University Hospital
SE-205 02 Malmö, Sweden

ISSN 1652-8220
ISBN 978-91-86871-31-4
Printed in Sweden by Media-tryck, Lund, 2011

“*-En obeskrivligt lättfattlig instruktionsbok...*”
ur Tv-serien Tornado

“-Vi vänder blad!”
Hans Majestät Konungen

Abstract

The aim of this thesis was to investigate aspects on detectability of simulated lesions (microcalcifications and masses) in digital mammography (DM) and breast tomosynthesis (BT). Perception in BT image volumes were also investigated by evaluating certain reading conditions.

The first study concerned the effect of system noise on the detection of masses and microcalcification clusters in DM images using a free-response task. System noise has an impact on image quality and is related to the dose level. It was found to have a substantial impact on the detection of microcalcification clusters, whereas masses were relatively unaffected. The effect of superimposed tissue in DM is the major limitation hampering the detection of masses. BT is a three-dimensional technique that reduces the effect of superimposed tissue.

In the following two studies visibility was quantified for both imaging modalities in terms of the required contrast at a fixed detection performance (92% correct decisions). Contrast detail plots for lesions with sizes 0.2, 1, 3, 8 and 25 mm were generated. The first study involved only an in-plane BT slice, where the lesion centre appeared. The second study repeated the same procedure in BT image volumes for 3D distributed microcalcification clusters and 8 mm masses at two dose levels. Both studies showed that BT needs substantially less contrast than DM for lesions above 1 mm. Furthermore, the contrast threshold increased as the lesion size increased for both modalities. This is in accordance with the reduced effect of superimposed tissue in BT. For 0.2 mm lesions, substantially more contrast was needed. At equal dose, DM was better than BT for 0.2 mm lesions and microcalcification clusters. Doubling the dose substantially improved the detection in BT. Thus, system noise has a substantial impact on detection.

The final study evaluated reading conditions for BT image volumes. Four viewing procedures were assessed: free scroll browsing only or combined with initial cine loops at frame rates of 9, 14 and 25 fps. They were viewed on a wide screen monitor placed in vertical or horizontal positions. A free-response task and eye tracking were utilized to record the detection performance, analysis time, visual attention and search strategies. Improved reading conditions were found for horizontally aligned BT image volumes when using free scroll browsing only or combined with a cine loop at the fastest frame rate.

Original papers and preliminary reports

This thesis is based on the following papers, hereafter referred to in the text by their Roman numerals:

I. *Dose dependence of mass and microcalcification detection in digital mammography: Free response human observer studies*
Ruschin M, Timberg P, Båth M, Hemdal B, Svahn T, Saunders RS, Samei E, Andersson I, Mattsson S, Chakraborty DP, Tingberg A.
Med. Phys. 2007; 34(2):400-407

II. *In-plane visibility of lesions using breast tomosynthesis and digital mammography*
Timberg P, Båth M, Andersson I, Mattsson S, Tingberg A, Ruschin M.
Med. Phys. 2010; 37(11):5618-5626

III. *Visibility of microcalcification clusters using breast tomosynthesis and digital mammography: a 4AFC human observer study*
Timberg P, Båth M, Andersson I, Mattsson S, Tingberg A, Ruschin M.
Manuscript submitted for publication in Med. Phys. 2011

IV. *Breast tomosynthesis image volumes are read more efficiently when displayed horizontally. A free-response study combined with eye tracking*
Timberg P, Lång K, Holmqvist K, Nyström M, Wagner P, Förnvik D, Tingberg A, Zackrisson S.
Manuscript submitted for publication in Acad. Radiol. 2011

Preliminary reports have been presented at the following meetings:

i. SPIE Medical Imaging, San Diego, USA, 11-16 February 2006. Timberg P, Ruschin M, Båth M, Hemdal B, Andersson I, Mattsson S, Chakraborty D, Saunders R, Samei E and Tingberg A. - **Potential for lower absorbed dose in digital mammography: A JAFROC experiment using clinical hybrid images with simulated dose reduction**, *Proc SPIE **6146**:341-350*

ii. SPIE Medical Imaging, San Diego, USA, 17-22 February 2007. Ruschin M, Timberg P, Svahn T, Andersson I, Hemdal B, Mattsson S, Båth M, and Tingberg A. - **Improved in-plane visibility of tumors using breast tomosynthesis**, *Proc SPIE **6510**:6510J.1-11*

iii. Third Malmö Conference on Medical Imaging, Malmö, Sweden, 25-27 June 2009. Timberg P, Andersson I, Förnvik D, Hemdal B, Mattsson S, Båth M, Tingberg A and Ruschin M. - **In-plane visibility of lesions using breast tomosynthesis**.

iv. SPIE Medical Imaging, Orlando, USA, 12-17 February 2011. Lång K, Zackrisson S, Holmqvist K, Nyström M, Andersson I, Förnvik D, Tingberg A and Timberg P. - **Can horizontally oriented breast tomosynthesis image volumes or the use of systematic strategy improve interpretation? An eye tracking and free-response human observer study,** *Proc SPIE **7966***:796606.1-12

v. SPIE Medical Imaging, Orlando, USA, 12-17 February 2011. Lång K, Zackrisson S, Holmqvist K, Nyström M, Andersson I, Förnvik D, Tingberg A and Timberg P. - **Optmizing viewing procedures of breast tomosynthesis image volumes using eye tracking combined with a free-response human observer study,** *Proc SPIE **7966***:796602.1-11

Abbreviations

2D	Two-dimensional
3D	Three-dimensional
AFC	Alternative forced-choice
AFROC	Alternative FROC
ANOVA	Analysis of variance
AGD	Average glandular dose
BT	Breast tomosynthesis
CC	Craniocaudal
d'	Detectability index
DM	Digital mammography
FOM	Figure-of-merit
FROC	Free-response receiver operating characteristics
JAFROC	Jackknife AFROC
LL	Lesion localization
LLF	Lesion localization fraction
MAFC	Multiple AFC
MLO	Mediolateral oblique
MTF	Modulation transfer function
NL	Non-lesion localization
NLF	Non-lesion localization fraction
NPS	Noise power spectrum
PC	Proportion of correct responses
ROC	Receiver operating characteristics
ROI	Region-of-interest
SFM	Screen-film mammography
SPR	Scatter-to-primary ratio

Contents

1 Introduction

Screen-film mammography (SFM) has widely been considered the most important breast imaging modality since its introduction. However, this technique still offers a limited sensitivity (Laming and Warren, 2000; Pisano et al., 2005; Poplack et al., 2000; Rosenberg et al., 2000) missing up to 30% of the breast cancer cases. Expectations were high that the introduction of digital mammography (DM) would lead to improvements in both image quality and diagnostic accuracy. However, only two out of ten studies comparing DM with SFM as screening modality showed a statistical significant advantage in favour of DM (Skaane, 2009).

One of the benefits of DM over SFM is its wider dynamic range with respect to dose, allowing operation in a quantum noise (stochastic poisson distributed fluctuations of X-ray intensity) limited region, relatively lower than SFM (Chawla et al., 2006; Hemdal et al., 2005; Hemdal et al., 2002; Huda et al., 2006). When considering a dose reduction, the benefit of reducing the risk of radiation induced breast cancer should be weighted against the risk of introducing noisier images and thus compromising diagnostic accuracy.

A major limitation of DM is the superimposition of tissue when the anatomy is projected down to a two-dimensional (2D) image (without depth resolution), potentially hampering detection of existing lesions or generating false findings suspicious for malignancy. To partially resolve this limitation a three-dimensional (3D) imaging approach called breast tomosynthesis (BT) has been proposed (Niklason et al., 1997). Experimental as well as clinical studies have shown BT to be better than DM, particularly for breasts with a high proportion of fibroglandular tissue (Andersson et al., 2008; Gur et al., 2009). An overview of local initial experiences with BT has recently been published (Tingberg et al., 2011).

Two frequent signs of breast cancer are masses and small calcifications (typically 0.1–0.5 mm) often referred to as microcalcifications and arranged in clusters. Perception studies under controlled conditions have shown that the effect of superimposed tissue is the main reason for decreasing the visibility of masses, whereas microcalcification clusters (and subtle characteristics of masses and surrounding tissue) are more sensitive to system noise (quantum noise and electronic noise) and thus relatively dose-

dependent (Bochud et al., 1999; Burgess et al., 2003; Burgess et al., 2001; Huda et al., 2006).

BT generates an extensive set of data compared to DM and the reading time is also longer (Good et al., 2008). In a screening situation a high throughput of examinations and an efficient workflow is crucial. The need for optimization of reading conditions for BT is obvious.

Currently, the standard viewing procedure for BT image volumes is free scroll browsing, but in many cases, the observer utilizes (or has the option to utilize) a cine loop to get a quick overview. How different frame rates of the cine loop are related to detection in BT image volumes and if there is a benefit of showing an initial cine loop have not yet been investigated.

The BT image volume could be displayed on a wide screen monitor in either vertical or horizontal position. The peripheral vision guides visual search (Banks et al., 1991; Engel, 1977; Kundel, 1975) and it has been confirmed in visual search tasks that the perceptual span is larger for horizontal than vertical searches (Anstis, 1974; Philips and Edelman, 2008). However, in radiology the traditional reading setting for a wide screen monitor is vertical orientation. The influence on efficiency and accuracy in interpreting BT image volumes horizontally has not yet been investigated. When estimating how BT image volumes are perceived, eye tracking can be utilized.

1.1 Objectives

The objectives of this thesis were:

- to investigate the effect of system noise on search-based detection of masses and microcalcification clusters in DM images using a free-response task (**Paper I**),
- to quantify the required contrast threshold (at a fixed detection performance) for different simulated lesion sizes based on the visibility in in-plane BT slices and DM images (**Paper II**),
- to compare visibility of 3D distributed masses and microcalcification clusters in reconstructed BT image volumes and DM images (**Paper III**),
- to evaluate how BT image volumes can be read efficiently, using a free-response study combined with eye tracking (**Paper IV**).

2 Scientific and technical background

2.1 Imaging modalities relevant for the current studies

2.1.1 Digital mammography

A widespread X-ray technique that has gained implementation in breast imaging is DM. Some of the major advantages are the convenient handling and archiving of the images and a large dynamic range with respect to exposure. DM images are formed by converting X-rays (transmitted through the breast), which are absorbed in a 2D detector, into digitized signal values, commonly referred to as pixel values (Figure 2.1). The main normal and abnormal tissue components of the breast (adipose, fibroglandular, tumor tissue and calcifications) have different attenuation (integrated energy dependent probability of possible interactions resulting in an energy absorption) of the X-rays. The result is a transmission map which can be transformed into a image by assigning a number of grey levels (Figure 2.2). The image can be presented on a dedicated monitor and processed to enhance tissue components adjusted for the human eye.

There are several detector principles that can be utilized, mainly categorized into direct or indirect conversion detectors (Mahesh, 2004; Noel and Thibault, 2004; Pisano and Yaffe, 2005; Rowlands, 2000). When utilizing direct conversion, X-rays are absorbed in a semi-conductor layer, creating electron-hole-pairs that are collected by an electrical field and stored into a thin film transistor array. In an indirect conversion detector the absorbed X-rays are first converted into visible light in a scintillator, then the light is collected in a photodiode, converting it into electrical charge and storing it. Finally each detector element is read out and digitized (to form an image). Other techniques that can be utilized are computed radiography (Rowlands, 2002) and direct photon counting detectors (Åslund et al., 2007).

The DM unit used in this work was a Siemens Mammomat Novation (Erlangen, Germany), containing a direct conversion a-Se flat panel detector measuring 24 cm × 29 cm and with a detector pixel size of 70 μm × 70 μm. The beam quality can be adjusted by varying the X-ray tube potential (25–32 kVp) and by using different anode/filter combinations; W/Rh or Mo/Mo. An appropriate beam quality is configured to meet the optimal operating range of the detector based on breast thickness and glandular content. During the examination, the breast is compressed and irradiated. In

the investigations included in this thesis, the beam quality was selected based on the breast thickness and the exposure was regulated based on the breast composition and thickness with an automatic exposure control. The average glandular dose (AGD) was 1.3 mGy in the study presented in **Paper I** and 0.8 mGy in the remaining studies for a standard breast (50 mm compressed breast thickness with 50% fibroglandular content) (Dance et al., 2000; Zoetelief et al., 1996.).

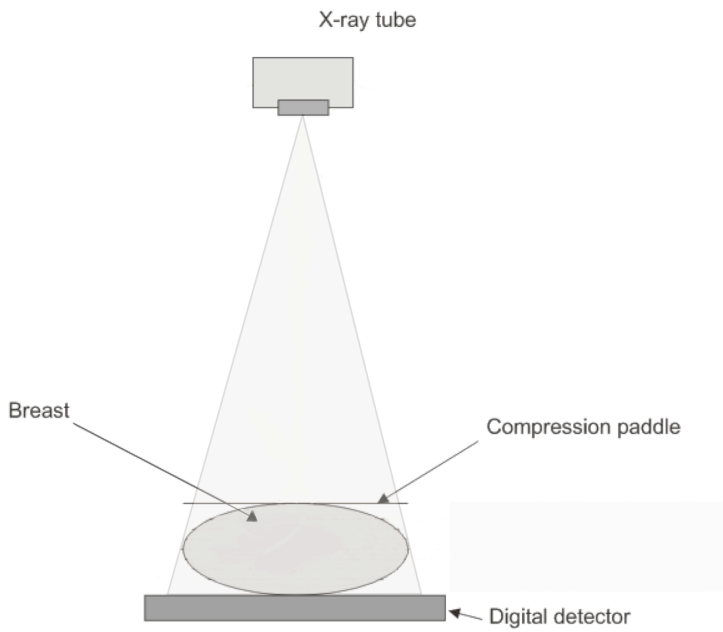

Figure 2.1 - Schematic illustration of a DM unit.

Figure 2.2 - DM image with bright dense areas representing mainly fibroglandular tissue, whereas the darker areas represent mostly adipose tissue.

2.1.2 Breast tomosynthesis

Breast tomosynthesis can be defined as the acquisition of a number of projection images at different angles from which slices parallel to the detector plane can be reconstructed (Figure 2.3). Typically, the X-ray tube moves in an arc over a limited angular span of ~10 to 50 degrees usually over a stationary detector, acquiring ~11 to 25 low dose projection images (Andersson et al., 2008; Bissonnette et al., 2005; Niklason et al., 1997; Reiser and Nishikawa, 2010). These images are reconstructed to form a 3D breast volume usually with 1 mm thick slices (Figure 2.4). In general, the absorbed dose is approximately twice that of a single DM image. There are several reconstruction algorithms that regulate signals, minimize noise and artifacts caused by sparse sampling and reconstruction parameter settings (Hu et al., 2008; Wu et al., 2004). It has been shown that the sensitivity of BT was superior over DM in selected patient groups (Andersson et al., 2008; Gur et al., 2009). However, other studies have been unable to demonstrate an advantage of BT over DM (Gennaro et al., 2010; Svane et al., 2011; Teertstra et al., 2010). The sensitivity combined with specificity

remains unknown in unselected clinical materials as well as the performance of BT as a screening modality. To the knowledge of the author, these issues will be investigated in two ongoing clinical screening trials in Malmö and Oslo (ClinicalTrials.gov id: NCT01091545; NCT01248546). Some of the major advantages are that BT can be operated at relatively low dose levels and provides high resolution slices in the plane parallel to the detector with improved depth resolution compared with DM.

The BT unit used in this work was a prototype based on the Siemens Mammomat Novation (Erlangen, Germany). The X-ray tube was modified to move continuously along the arc acquiring 25 projection images evenly distributed over 50 degrees over a stationary flatpanel detector with a detector pixel size of 85 μm × 85 μm that enables fast read out (Bissonnette et al., 2005). The exposure was synchronized with detector read out. The AGD was approximately 1.6 mGy for a 50 mm standard breast. In this work a generalized filtered back projection reconstruction method was used with filters designed for sparse sampling (Hu et al., 2008; Lauritsch and Haerer, 1998; Mertelmeier, 2006; Orman et al., 2006; Zhao et al., 2009).

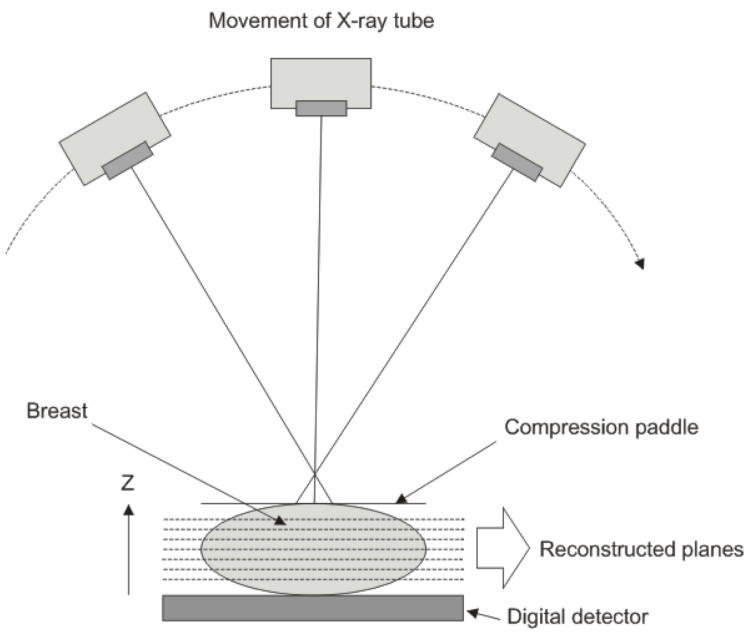

Figure 2.3 - Schematic illustration of a BT unit.

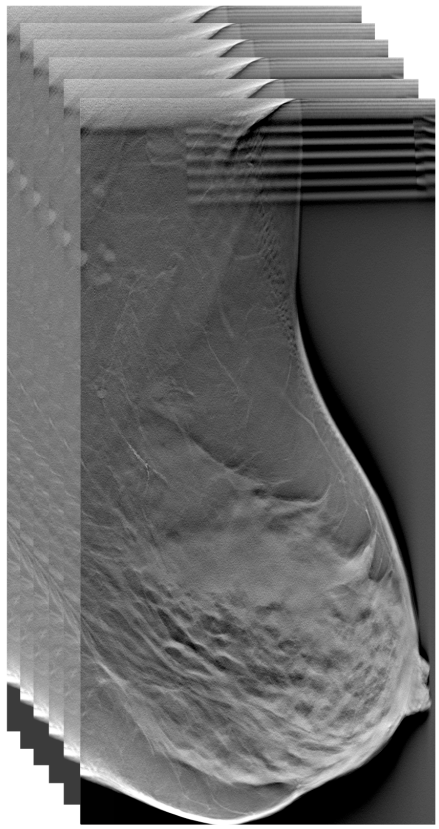

Figure 2.4 - An example of a stack of BT slices.

2.2 Perception metrology

2.2.1 The free-response task

The current golden standard for evaluating imaging system performance is receiver operating characteristics (ROC) (Metz, 1986; Metz, 2000). It has however not been used in this thesis, since it does not handle multiple suspicious regions/lesions or information about their localization. Instead, to quantify detection or diagnostic performance, a free-response task was used allowing the observer to freely locate and mark suspicious regions in the images. The findings (single or multiple) are rated according to a confidence level based on the observer's decision certainty. If a mark is within the determined lesion region it is defined as a lesion localization (LL), else it is

a non-lesion localization (NL). The establishment of the truth is crucial as the truth is *a-priori* unknown to the observer and a prerequisite when conducting free-response tasks.

An established way of presenting the free-response task performance is to generate a FROC (Free-response Receiver Operating Characteristics) curve and calculate the area under the curve referred to as figure-of-merit (FOM) (Bunch PC et al., 1978). The FROC curve is generated by plotting the lesion localization fraction (LLF) versus non-lesion localization fraction (NLF), where LLF is LL divided by the total number of lesions and NLF is NL divided by the total number of images. Since the NLF depends upon the number of NL divided by the total number of images, the abscissa in the plot can extend indefinitely, leading to a less suitable FOM ($0 \leq FOM \leq \infty$) metric.

Another possibility is the Alternative FROC (AFROC) curve, where the relationship of LLF versus false positive fraction (FPF) is plotted (Chakraborty and Winter, 1990). The FPF is the number of normal images incorrectly identified as abnormal images divided by the total number of normal images. The FOM representing the area under the AFROC curve in this case is within square unity ($0 \leq FOM \leq 1$). It is the probability that lesions are rated higher on abnormal images than on normal images.

Jackknife AFROC (JAFROC) is a resampling method used in **Paper I** and **IV** to analyze multiple readers and cases in free response task data (Chakraborty and Berbaum, 2004). The statistical power (the probability of rejecting the null hypothesis when it is false) of this method has been reported to be exceptional for free-response tasks (Chakraborty, 2008). The JAFROC FOM is the probability that a LL rating (on abnormal images) exceeds all NL ratings (on normal images). It is defined in Equation 2.1:

$$\begin{cases} FOM = \frac{1}{N_N N_L} \sum_{i=1}^{N_N} \sum_{j=1}^{N_L} \psi(X_i, Y_j) \\ \psi(X,Y) = \begin{cases} 1.0 \; if \;\; Y > X \\ 0.5 \; if \;\; Y = X \\ 0.0 \; if \;\; Y < X \end{cases} \end{cases} \qquad \text{Eq. 2.1}$$

where X_i is the highest NL rating for case i and Y_j is the LL rating for lesion j. N_N and N_L are the total number of normal cases and lesions, respectively. ψ is the function that involves the comparisons of X and Y. In most cases

free-response tasks involve several cases and observers, when comparing different conditions or modalities. In the jackknife step, pseudo-values are created by sequently removing a case (repeated for each condition or modality and observer) and recalculating FOM, creating a pseudo matrix. This matrix is analyzed by using a mixed model analysis of variance (ANOVA) that yields a p-value for rejecting the null hypothesis that the observer-averaged FOMs are identical. Furthermore, it provides confidence intervals for the difference in FOM of the investigated conditions (Chakraborty, 2010).

2.2.2 The alternative forced choice method

In special tasks involving detection or discrimination of signals in noisy backgrounds under more controlled conditions than in a free-response task, the alternative forced-choice (AFC) method could advantageously be employed (Burgess, 1995; Burgess et al., 2001). The experiment is fast to perform as the observer's search is usually limited to small regions (segmented images) and no reports of decision certainty is required. The cost- and time-consuming involvement of radiologists is not needed as no clinical experience is required for the task. However, a limitation of this method is that it does not reflect a clinical realistic task (including both perception and interpretation: search; detection; and classification) and that sensitivity and specificity pairs cannot be reported.

In **Paper II** and **III** a MAFC (M is the number of alternative locations) detection task has been utilized as suggested by Burgess (Burgess, 1995). An example of a 4AFC is shown in Figure 2.5. In this case, the observer is presented with four random images with overlay of concentric circles. In one of them is a signal stimulus randomly inserted. Presented above these images is a cue (concentric circle and signal) to guide the observer of both the signal stimulus (size, shape, distribution) and location. The observer is forced to choose the region most likely holding the signal. The proportion of correct responses (PC) is then determined or, alternatively, a detectability index (d') is calculated. Chance performance is given by PC = 1/M for equal prior probabilities. The detectability index is a common measure referred to as the observer's ability to discriminate between signal-present locations (correct decisions) and noise-present locations (incorrect decisions) as characterized by two probability density functions (Myers, 2000). It is especially useful since d' is linearly related to the contrast of the signal stimulus, and can be used to generate contrast-detail plots (Figure 2.6). The transformation of PC to d' is presented in Equation 2.2 assuming statistically

independent responses and normally distributed probability density functions with equal variances:

$$PC(d', M) = \int_{-\infty}^{+\infty} \phi(x-d') \, [\Phi(x)]^{M-1} dx \qquad \text{Eq. 2.2}$$

$$\phi(x) = \frac{1}{\sqrt{2\pi}} e^{-\frac{x^2}{2}}, \qquad \Phi(x) = \int_{-\infty}^{x} \phi(y) dy$$

where ϕ is the probability density function for the stimuli present decision variables and Φ is the cumulative distribution function for the stimuli-absent function (Eckstein et al., 2000).

Usually in 4AFC tasks the contrast threshold is determined approximately at d' = 2.5 (PC ~92%). This is a consequence of having a minimum coefficient of variation of the d' at this point since PC is binomially distributed (Burgess, 1995). The low contrast thresholds reported are often unrealistic for clinical trials such as in the free-response task. Since the 4AFC task involves limited search area, cues and knowledge about the signal characteristics, the contrast would need to be increased in a free-response task.

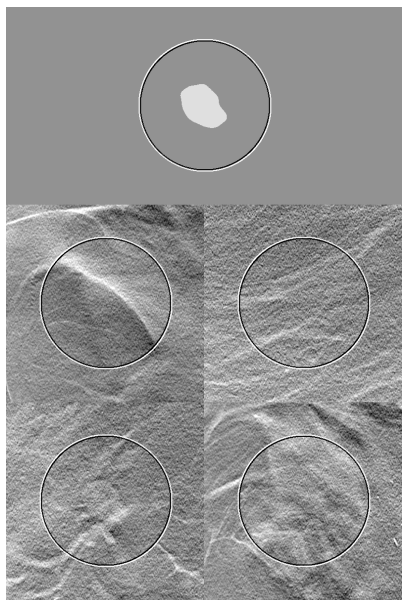

*Figure 2.5 - A 4AFC BT case from **Paper II**. The key signal is presented on top, indicating the shape of the inserted 8 mm mass present at bottom left.*

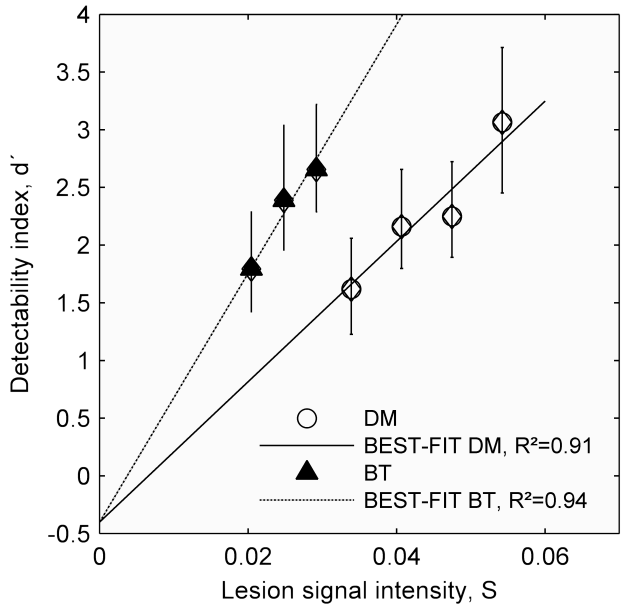

*Figure 2.6 - An example from **Paper II** of a plot of d' versus lesion signal intensity (i.e. contrast) for a 8 mm mass in in-plane BT slices and DM images. The error bars are 95% confidence intervals.*

A statistical resampling method called bootstrapping was used in **Paper II** and **III** in order to assemble confidence intervals of d' differences of investigated conditions or modalities (Efron, 1982; Efron and Tibshirani, 1994). This is particularly useful when samples or observers are limited. In this method, a bootstrap is performed by randomly extracting a new sample from the collected data from which a metric (e.g. d') is calculated. By repeating this many times, a distribution of d' values is generated, providing an estimate and requested percentiles, hence the confidence interval for either the estimate or differences of conditions or modalities is created.

2.2.3 Eye tracking

When analyzing how BT image volumes are visually attended and searched, eye tracking can be utilized. It consists of an infrared camera that tracks eye movements, and calculates gaze position using image processing and geometrical calculations (Holmqvist et al., 2011). The eye tracker records the gaze position 50–2000 times per second with an accuracy down to 0.2

degrees of visual angle. The visual field consists of the central high resolution foveal vision (about 2 degrees), parafoveal vision (2-5 degrees) and the low resolution peripheral vision (≤ 240 degrees) (Kundel, 1975). The foveal vision is usually tracked (along with the size of the pupil). The peripheral vision is useful in an initial global overview stage and as guidance to direct a local focused search (Kundel, 1975; Kundel and Nodine, 1975; Kundel et al., 1991). It is however difficult to track where attention is located in the periphery. Experienced observers also appear to use the peripheral vision more effectively than novices (Kundel, 1975).

Eye tracking can be used as an aid to understand observers' visual attention and search strategies. In radiology, it has been used mainly to analyse how radiologists read mammograms (Kundel et al., 2007; Kundel et al., 2008; Mello-Thoms, 2006a; Mello-Thoms, 2006b; Mello-Thoms et al., 2005) and chest radiographs (Kundel et al., 1991; Litchfield et al., 2010; Manning et al., 2006; Manning, 2004). Visual attention (spatial locus of intake and processing) acts slightly before the eye does (< 250 ms) (Deubel, 2008), and is triggered by the target's contrast, size, shape, sharpness and also higher cognitive factors such as memory, task etc.

Some common eye tracking measures used in this work are dwell time, dispersion, transitions and region-of-interest (ROI) entry time (Holmqvist et al., 2011). The dwell time is the duration of one visit to a specific ROI from entry to exit. A minimum dwell time of 100 ms was referred to as a hit. If revisits are included, the total dwell time is the summed durations of all visits. The dispersion quantifies the distribution of the eye tracking data over the ROI. When the observers are presented with a stimulus of interest, it is sometimes desirable to record the entry time and transition length (position of gaze at lesion onset to ROI hit) from the trial start or stimulus appearance to the ROI visitation. The steps made in a transition involve perception, interpretation, decision making, and execution. Traditional measures of fixation durations and saccade lengths were not used since there exist no robust calculation methods for dynamic presentations.

In **Paper IV**, it was hypothesized that a higher proportion of dwell time is beneficial for getting ROI attention and potentially leading to better detection performance. Longer transition lengths are indicative of utilizing more of the peripheral visual field as guidance to foveal search (Ojanpaa et al., 2002; Philips and Edelman, 2008). The peripheral visual field has been shown to dominate in the horizontal extension and it is considered preferable to read horizontally extended objects (Anstis, 1974), especially in

dynamic image presentations (e.g. BT image volumes) (Abrams and Christ, 2003; Franconeri and Simons, 2003; Megaw and J., 1979). Theoretically, viewing horizontally oriented presentations of BT image volumes makes the reading more efficient since the extension of the visual field is better aligned with the viewing area of the monitor. Such alignment seems particularly useful when viewing dynamically presented BT image volumes where abnormalities appear abruptly in the peripheral part of the visual field. Such abrupt onsets are known to capture attention (Abrams and Christ, 2003), and thus guide the eyes to potential lesion locations. This might be reflected in a faster total analysis time and a shorter entry time. Regarding entry time it was hypothesized that a shorter entry time indicates faster detection. It was also hypothesized that the dispersion decreases with increasing cine loop speeds. Potentially, the time constraint when viewing fast-moving stimuli could make eye movements less efficient, compared to a strategy where long fixations are used to monitor the stimulus (Moraal, 1975).

The eye tracking unit used in this work (**Paper IV**) was a tower mounted SMI HiSpeed 240 (SensoMotoric Instruments, Germany) with a sampling frequency of 240 Hz and a measured average accuracy of 0.3 degrees of visual angle (Figure 2.7). The recording computer was running an iViewX 2.2 software in pupil-corneal reflection mode (www.smivision.de). A special ViewDEX software, mainly used for presenting images and tracking observers' marks and ratings, was developed and synchronized to communicate with the recording computer (Figure 2.8) (Börjesson et al., 2005; Håkansson et al., 2010). No general oculomotor statistics (e.g. fixation duration and saccade length) were given as the analysis were made on raw eye tracking data.

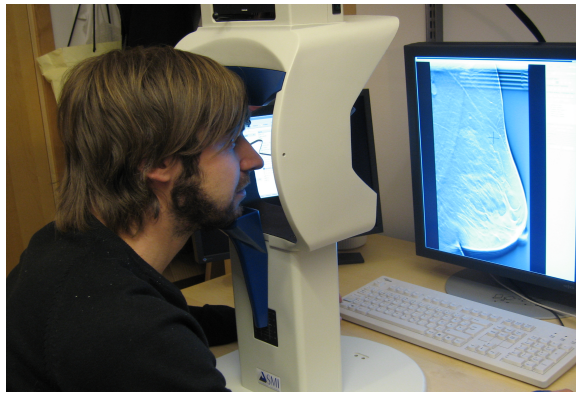

Figure 2.7 - Setup of the SMI HiSpeed 240 eye tracking unit. The BT image volumes were presented on a 5 mega-pixel flat panel EIZO SMD 21510 wide screen monitor (oriented in vertical position).

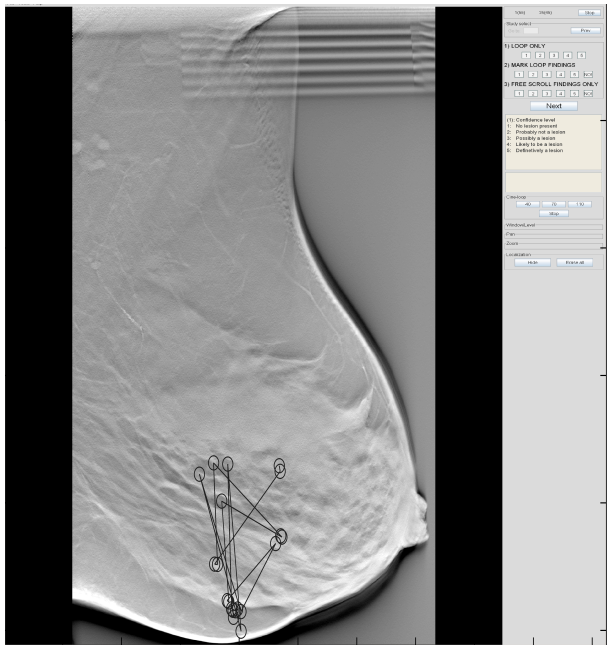

Figure 2.8 - Eye tracking data overlayed on an BT slice presented in ViewDEX.

2.3 Hybrid images

2.3.1 Lesion simulation and insertion method

Detection involved in the free-response and AFC task is related to target properties such as size, shape, complexity, contrast, edges and human factors such as internal decision thresholds (depending on experience, knowledge, expectancies and motivation). Additionally, detection in clinical images involves targets embedded in anatomic backgrounds. In order to control the ground truth (position, lesion type, size, shape and contrast), it is sometimes desirable to create hybrid images, especially under target conditions with visibility at the perception threshold (representing the major limitations of the investigated conditions). A hybrid image can be created by using a normal image, into which one or several simulated lesions are inserted and/or manipulated by changing imaging properties.

In **Paper I–IV**, lesions were simulated to represent irregularly shaped masses and microcalcifications (single or distributed as clusters), both frequently encountered breast abnormalities (Figure 2.9). Signal templates of the lesions (a 2D signal plane parallel to the detector), based on anatomical characteristics of real lesions, were developed in collaboration with a group at Duke University (Ruschin et al., 2005). Their realistic appearance was verified by radiologists at Duke University (Saunders and Samei, 2004; Saunders et al., 2006). The signal templates could be adjusted to any desired size (0.1–25 mm), and optionally filtered with the detector modulation transfer function (MTF) (**Paper I**). The MTF is a measure of the spatial frequency response (i.e. signal modulation) of the image system. The clusters consisted of 15–42 randomly distributed microcalcifications. The simulation and insertion process was based on previous studies (Lefebvre et al., 1994; Ruschin et al., 2005) described in **Paper I** and **III**. Lesions inserted in BT volume images need to have a 3D distribution and therefore need to be projected down at different angles into the projection images and subsequently used as input in the reconstruction (**Paper II–IV**). This was achieved by extending parallel planes of the signal template with decreasing dimensions forming an ellipsoid. The voxel size of the 3D lesions (0.01–0.03 mm^3) needs to be sufficiently small to eliminate sampling artifacts.

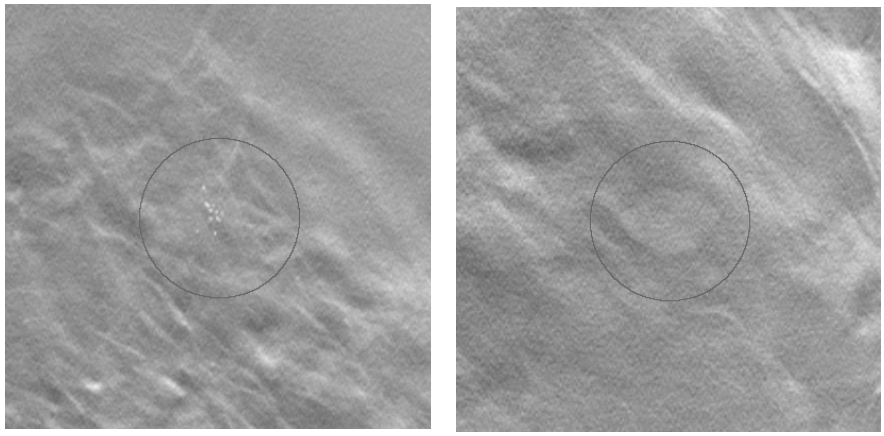

Figure 2.9 - Segments of reconstructed BT slices holding simulated lesions. To the left is a microcalcification cluster and to the right is a mass as used in ***Paper III*** *and* ***IV****.*

In the insertion step, the geometrical and detector properties need to be accounted for along with the physical properties (related to X-rays) of the simulated lesion. The only detector property taken into account was the aperture. The 3D lesions were projected onto the detector plane for every projection angle by mapping each voxel to detector element (i,j). This yielded a set of signal thickness images $t_k(i,j)$ corresponding to the integrated thickness of the lesion along the X-ray trajectories for each projection angle k. These images could then be inserted into linear clinical background images, $\mathrm{Im}_{O,k}(i,j)$, to form hybrid projection images, $\mathrm{Im}_{H,k}(i,j)$,

$$\mathrm{Im}_{H,k}(i,j) = \mathrm{Im}_{O,k}(i,j)e^{-\frac{t_k(i,j)\Delta\mu}{(1+SPR)}} \qquad \text{Eq. 2.3}$$

where $\Delta\mu$ is the difference in the attenuation coefficient between the existing breast tissue and the added lesion and the term $t_k(i,j)\Delta\mu$ is the projected lesion signal intensity map, and SPR is the scatter-to-primary ratio (SPR is only corrected for in **Paper II**–**IV** and the expression in Equation 2.3 is only valid for $t_k(i,j)\Delta\mu \ll 1$). A limitation is that the method is not replacing existing tissue or accounting for interacting background tissue upon impact.

As the signal has unique spatial variations, the contrast of the lesion S_{RMS} is defined as the root mean square of the signal intensity map of the central BT projection image or DM image (k = 0) and represents a relative increase in the total attenuation of the primary X-rays (Equation 2.4).

$$S_{RMS} = \sqrt{\frac{1}{MN}\sum_{i=1}^{M}\sum_{j=1}^{N}(t_{(k=0)}(i,j)\Delta\mu)^2} \qquad \text{Eq. 2.4}$$

where M and N are total number of detector rows and columns, respectively. In this way, the value of $\Delta\mu$ that would result in the desired value of S_{RMS} for a given lesion was determined. The same $\Delta\mu$ was then used for all the projection angles.

There are several ways of determining the contrast threshold suitable for the detection task. Usually, one determines the contrast by conducting a pilot study and finding out the observer's performance and adjusting accordingly (**Paper II**–**IV**). If it involves a clinical task, it should be at realistic contrast thresholds reflecting the characteristics of the population of interest. Another way, although more subjective, is by simply adjusting the contrast until a desired visibility is reached according to an expert panel, usually experienced radiologists (**Paper I**).

2.3.2 Dose reduction simulation routine

In **Paper I**, a dose reduction simulation routine was customized for DM images based on a previously described algorithm (Figure 2.10) (Båth et al., 2005; Svalkvist and Båth, 2010; Timberg et al., 2006). BT projection images can also be used, but has not been part of any projects yet. In this routine, quantum noise (stochastic poisson distributed fluctuations of X-rays) was simulated and the linear original images were scaled as to be acquired on a detector operating at a quantum noise limited range. The simulated added noise (both uncorrelated and correlated to the original image) was based on measured system noise properties, measured on flat field images collected at the original and simulated dose level, including both quantum noise, electronic noise and structural defects in the detector as described by the noise power spectrum (NPS). The NPS holds the various spatial frequencies that comprise the noise in an image. A prerequisite was a constant MTF at each dose level.

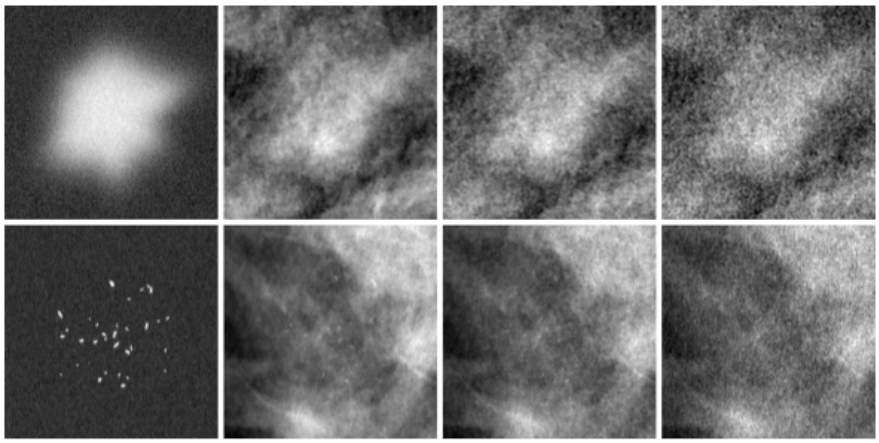

*Figure 2.10 - Simulated lesions (mass in top row and microcalcification cluster in bottom row) inserted into DM images, forming hybrid images at the 100% and simulated 50% and 30% dose level in consecutive order (**Paper I**).*

An alternative way, as used with BT volume images, is to simply remove projection images prior to the reconstruction as described in **Paper II–IV**, approximating a lower dose acquisition.

3 Summary of the papers

3.1 Paper I: Dose dependence of mass and microcalcification detection in digital mammography: Free response human observer studies

In **Paper I,** detection performance was evaluated for four radiologists reading DM images at different dose levels (100%, 50%, 30% of an AGD of 1.3 mGy) using JAFROC. The lesions involved were microcalcification clusters (36 individual calcifications, each ~0.26 mm) and irregular masses (9 mm), inserted randomly into ~40% of 90 normal images selected from a population based mammography screening program (forming hybrid images). The hybrid images were then dose reduced according to the dose reduction simulation routine (with additional image processing), yielding a set of 270 images, divided randomly into 3 viewing sessions. In the free-response task the radiologists used ViewDEX and were allowed to mark as many locations as desired and to provide required confidence ratings. The reader-averaged FOM is presented in Figure 3.1. No statistical significant

difference was found for the masses ($p = 0.19$). However, the detection of microcalcification clusters was dose-dependent with a statistically significant difference in FOM ($p < 0.0001$) between any pairs of dose levels.

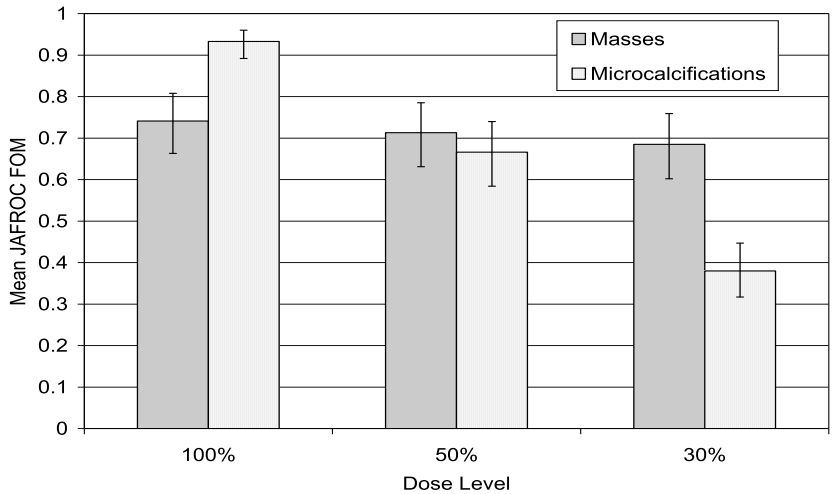

Figure 3.1 - Reader-averaged FOM including 95% confidence intervals for masses and microcalcification clusters.

3.2 Paper II: In-plane visibility of lesions using breast tomosynthesis and digital mammography

In **Paper II,** lesion visibility was studied in segmented DM images and reconstructed in-plane BT slices (central slice of the lesion). A series of 4AFC trials (60 cases each) were set up to quantify human detection performance of randomly shaped irregular masses (size: 0.2, 1, 3, 8 and 25 mm), and to subsequently quantify the required contrast thresholds. The dose levels were approximately the same (i.e. standard AGD of 0.8 mGy). Additionally (as indicated by the dose-dependence in **Paper I)**, the dose was also doubled for the 0.2 mm lesion, as used in the clinical BT standard acquisition protocol. Four medical physicists participated. A contrast-detail plot was generated by determining the contrast threshold (d' = 2.5) for each size and bootstrapping the corresponding confidence intervals (Figure 3.2).

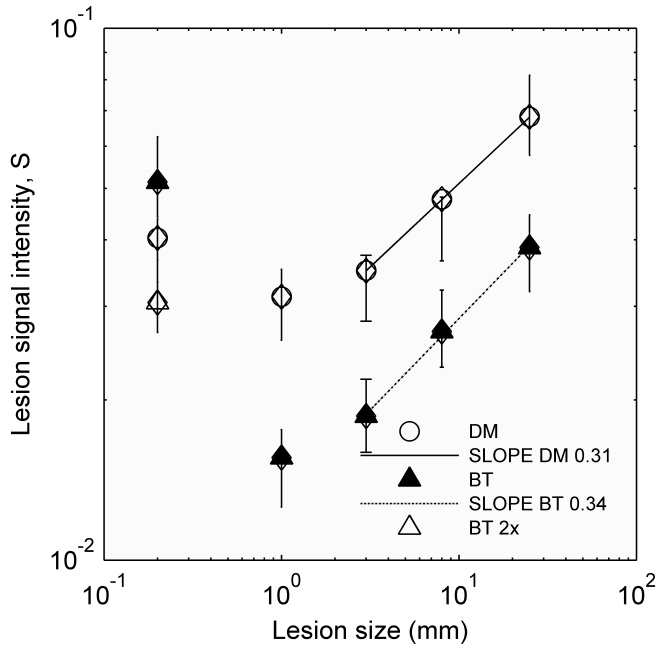

Figure 3.2 - Contrast-detail plot including 95% confidence intervals showing the required contrast threshold (lesion signal intensity) needed for different lesion sizes to achieve a d' of 2.5 for BT and DM. Note that for 0.2 mm lesions an extra dose level is present for BT.

The results indicate that lesions 1 mm or larger have a higher visibility in in-plane BT slices than in DM images, indicating that the effect of the superimposed tissue is substantially reduced in BT. For these sizes the contrast threshold is increasing with size. However, as seen in Figure 3.2, a higher contrast threshold is required for the 0.2 mm lesions. These lesions had a higher visibility in DM images, when compared at the same dose level. The visibility was improved when the dose was doubled for BT, indicating that the effect of quantum noise dominates over the effect of projected anatomy for this lesion size.

3.3 Paper III: Visibility of microcalcification clusters and masses in breast tomosynthesis image volumes and digital mammography: a 4AFC human observer study

Paper III is a continuation of **Paper II** using the same basic 4AFC setup to investigate the visibility of 3D distributed microcalcification clusters (15 ×

0.2 mm) and masses (8 mm) in dynamic presentations of BT image volumes and in DM images. The same observers participated using the same clinical images but now including 29 BT slices. The slices were presented sequentially at a fixed frame rate at 5 fps. As an aid to the observer, cues were given as 2D and 3D distributed signals and concentric circles. The modalities were compared at approximately the same dose levels (i.e. standard AGD of 0.8 mGy) (Figure 3.3). The BT volumes were also compared at twice the dose. The required contrast threshold (at d' = 2.5) for masses was approximately a factor two higher for DM images compared to in BT image volumes at both dose levels. For the microcalcification clusters the contrast threshold was higher for BT image volumes than for DM images at both BT dose levels, with a statistically significant difference in the required contrast threshold at the same dose level. The results indicated a dose dependence for the detection performance in BT image volumes for detection of microcalcification clusters.

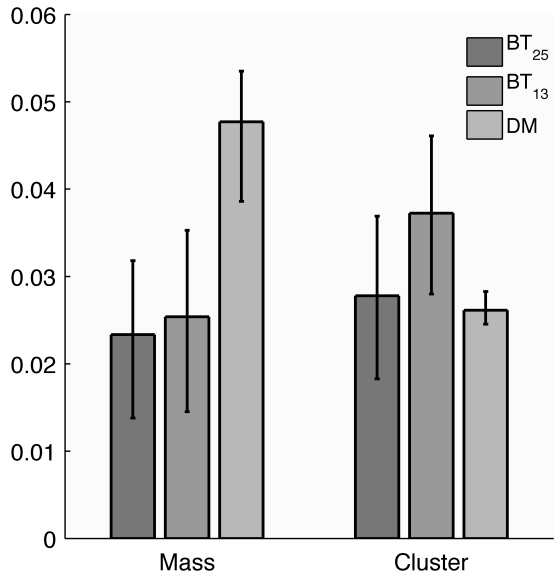

Figure 3.3 - Bar plot including 95% confidence intervals showing the required contrast threshold (lesion signal intensity) needed for microcalcification clusters and 8 mm masses to achieve a d' of 2.5 in BT image volumes and DM images. Note that BT has two dose levels BT_{25} and BT_{13} referring to the total number of projection images that were used in the reconstruction.

3.4 Paper IV: Breast tomosynthesis image volumes are read more efficiently when displayed horizontally. A free-response study combined with eye tracking

In **Paper IV**, four different viewing procedures and two presentation modes were evaluated in terms of detection performance, time efficiency and visual attention and search as part of improving BT reading conditions. The viewing procedures consisted of free scroll volume browsing only, and combined with initial cine loops at three different frame rates (9, 14 and 25 fps) terminated upon request. The presentation modes consisted of vertically and horizontally displayed BT image volumes (Figure 3.4). Fifty-five normal BT image volumes in MLO view were collected. In these, simulated 3D distributed lesions (20 masses and 20 microcalcification clusters) were randomly inserted, creating four unique image sets for each viewing procedure used in each presentation mode. Two radiologists and two medical physicists interpreted the cases in a random order. Their task was to locate a lesion, mark and assign a rating on a five level confidence scale. The detection performance was analyzed using JAFROC. Time efficiency, visual attention and search were investigated using eye tracking. In summary, no statistically differences in detection performance (FOM of 0.75 to 0.86) were found for any reading conditions. Horizontally oriented BT image volumes were read faster than vertically oriented when using free scroll browsing only (median time of 25 s vs 30 s) and when combined with fast cine loop (median time of 24 s vs 34 s). Cine loops at slow frame rates were ruled out as inefficient. Finally, faster cine loops leads to shorter entry times. More detailed results for each measure is presented in **Paper IV**.

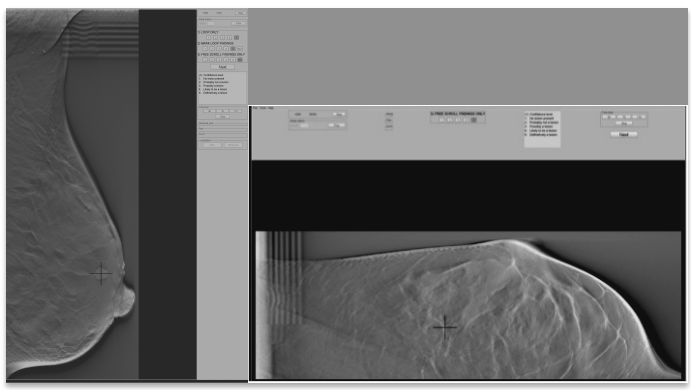

Figure 3.4 - Two presentation modes: vertically and horizontally.

4 Discussion and conclusions

The main results of **Paper II–III** indicate that the visibility of lesions larger than 1 mm is superior on BT compared with DM. The opposite is true for the 0.2 mm lesions and microcalcification clusters, i.e. better visibility on DM compared with BT at the same dose level. These results are in accordance with the hypothesis that the effect of superimposed tissue is the dominant image degrading factor for larger lesions, while system noise dominates for smaller lesions (microcalcifications). As shown in Figure 3.2, the positive slope in the contrast-detail plot for lesions above 1 mm predicts that a higher contrast threshold is required as lesion size increases in both BT and DM images. A substantially higher contrast threshold is needed for the 0.2 mm lesions. These results are in accordance with previous studies (Bochud et al., 1999; Burgess et al., 2001), which also showed that the opposite applies to lesions inserted into homogeneous images with just system noise. In that case the contrast-detail plot would have a negative slope. The effect of superimposed tissue is reduced by the improved depth resolution in BT (Reiser and Nishikawa, 2010). The system noise can be reduced by increasing the dose. However, when a dose increase is considered, the effects of improved image quality have to be weighed against the potential harm of the increased radiation exposure.

Another factor influencing the detection of microcalcifications is the fact that a cluster is distributed in several slices. Thus, frame rate and slice thickness may play a role. The results in **Paper IV** indicate that a higher frame rate and free scroll browsing may be superior to the fixed frame rate used in **Paper III**. Possibly, the observer has an increased ability to integrate 3D distributed stimulus over time in a short term memory at a certain frame rate.

Hybrid images were utilized in all studies, which may not completely reflect the clinical situation. However, this has to be viewed in the perspective of the difficulty of obtaining appropriate abnormal cases with known truth, ethical considerations regarding radiation exposures and time-cost issues. It is also difficult to find masses on the threshold of human perception. The advantage of hybrid images is the possibility of making relative comparisons with common hybrid images for all tested conditions. Further advantages of using hybrid images are fully controlled conditions, with the possibility to create any relevant realistic case. Using only two lesion types

leads to lower variability of the cases but does not fully reflect the morphologic spectrum of breast cancer.

A limitation of the used lesion simulation method is that it does not take into account the X-ray spectrum or the detector signal spread other than the aperture MTF. (The geometric properties of the simulation insertion method were assumed to be similar to the effect of the MTF aperture.) Regarding the contrast, a more realistic contrast threshold would be encountered if the lesion would grow (expansion of the lesion profile) with the same attenuation coefficient of the tissue rather than a relative increase in $\Delta\mu$ depending on the S_{RMS}. For future projects, a more refined lesion simulation method is desired, to mimic other lesion types.

The 4AFC task represents an experimental situation, not a true clinical search based task. However, it can be used to predict performance in a more clinically realistic search based task when taking into account the search area and the observers' inherent spatial imprecision to localize the lesions (Bochud et al., 2004; Burgess et al., 2001). A limitation in **Paper II** was that a single 0.2 mm microcalcification was viewed only in one slice (in-plane), whereas microcalcification clusters are 3D distributed over several slices. However, as investigated in **Paper III**, similar results were reached for the microcalcification clusters under 3D viewing conditions. **Paper III** still has the previously mentioned limitations of a 4AFC task regarding direct clinical implication. In relation to a search-based free-response task, more contrast would be needed to maintain a similar detection performance. Furthermore, more contrast would be needed if the observers are not provided with cues such as the size and shape of the lesions. In **Paper IV,** the contrast of the lesions had to be increased to be detectable when searching through entire BT image volumes. An estimated search factor related to the required contrast was derived from a free search model (Burgess et al., 2001) in breast images, indicating that about five times more contrast is needed compared to a two-alternative forced-choice task for 8 mm lesions. For this particular detection task in BT image volumes, this factor was increased to seven times for masses and five times for microcalcification clusters. All images in **Paper II** and **III** are currently used in projects involving model observers to objectively characterize influences of BT imaging parameters.

All studies involved detection tasks solely, without assigning a probability of malignancy. In a clinical situation, radiologists need to review the images, recognize, interpret and make decisions, consequently affecting the

outcome. Explanations of false negative findings due to search errors, recognition errors, and decision errors were out of the scope. For these reasons the results have to be confirmed in clinical populations.

In general, results from experimental studies are not immediately applicable to the clinical situation. The superior detectability of lesions larger than 1 mm should result in a higher sensitivity of BT to detect breast cancer, which is corroborated by some experimental clinical studies (Andersson et al., 2008; Gur et al., 2009) but not by others (Gennaro et al., 2010; Svane et al., 2011; Teertstra et al., 2010). **Paper II** and **III** showed worse detectability of microcalcifications in BT compared with DM at identical dose levels. However, the practical implications of these results have to be tested in large scale clinical studies of symptomatic as well as asymptomatic women and the efficacy in terms of sensitivity and specificity pairs, stage distribution, and time-cost issues have to be assessed and compared with DM.

Regarding the differences in FOM between the reading conditions in **Paper IV**, the study would require a substantial sample size to demonstrate statistically significant differences, which would be both cost- and time-consuming. Significant differences were not expected to be possible to demonstrate due to a large sources of variance. Any existing difference in FOM would probably be of minor importance from a clinical perspective since the observers are viewing the same cases and are allowed to free scroll during all conditions. Instead, the main focus was on time efficiency and visual attention and search.

A horizontal presentation of BT image volumes substantially reduced the total analysis time, in particular for free scroll browsing and combined with fast cine loop speed. In that way, images are better aligned with the human visual field, which has a wider extension horizontally than vertically (Banks et al., 1991; Engel, 1977). Peripheral vision can thus be used more efficiently to localize lesions in the BT image volumes, in particular for the BT image volumes in the dynamic presentations where lesions abrupt onsets are known to capture attention (Abrams and Christ, 2003; Franconeri and Simons, 2003) and thus attract the observers' gazes. Therefore, it should be emphasized that the real benefit lies in viewing dynamic images rather than stationary images like 2D mammograms. Performance and time efficiency will most likely improve with observers more experienced in reading BT image volumes horizontally.

The constellation of the observers may also be discussed in **Paper IV**. Since BT is a new modality, breast radiologists have not yet received thorough experience in reading BT cases. The imaged object is not presented in the same way as on a mammogram. These were the reasons along with practical issues why observers with limited experience in reading mammograms and BT image volumes were included. It has been shown that experienced mammographers detect most breast lesions by global recognition within 25 s in mammograms, where less experienced observers take longer time and that prolonged search increases the risk of error (Nodine et al., 2002). It would be interesting to include experienced breast radiologists and also to plot cumulative case decisions as function of time for all reading conditions.

The cine loop may provide a better and faster global overview of possible suspicious regions, and could speed up the following free scroll browsing. The observers spent surprisingly little time with the slow cine loop, and instead carried on with free scroll browsing, perhaps in an effort to find the relevant structures as quickly as possible. Relatively short time was also spent in the cine loop at medium and fast cine loop speeds, but is in this case possibly indicative of attracting quicker visual attention. The time spent in the cine loop was about twice the time for the normal cases compared to the abnormal cases. The observers were most likely biased due to higher lesion prevalence than in a screening situation and that only one lesion was present in the abnormal cases. In a screening situation the majority of the cases are normal, and the total analyze time of these must be emphasized. However, the normal cases were not truly read as in a screening situation, as mentioned earlier. The intention is to proceed with an additional study based on the most promising reading conditions.

The transition lengths were longer for masses than for microcalcification clusters. Possibly, masses generate stronger transient onsets in dynamic presentations, and therefore attract attention better. However, this could also be since the microcalcification clusters require a different, more systematic search strategy using shorter saccades. Regarding total dwell time and transition lengths, no statistically significant differences between any conditions were found. The results indicated that entry time was shorter when utilizing the cine loop than in free scroll. Although if a faster frame rate would be beneficial, it is still unclear when decisions are made. The entry time for all conditions was short. The free scroll browsing procedure was statistically significantly longer and it took more time to allocate the microcalcification clusters compared to the masses. Regarding dispersion, the data revealed no obvious correlation between dispersion and frame rate.

Conclusions according to the objectives of the thesis:

- *The effect of system noise on search-based detection of masses and microcalcification clusters in DM images using a free-response task* (**Paper I**). Lowering the present dose level by a factor of two compromised the detection of microcalcification clusters but had less effect on mass detection. Therefore, caution should be exercised when proposing dose reduction strategies.

- *The required contrast threshold (at a fixed detection performance) for different simulated lesion sizes based on the visibility in in-plane BT slices and DM images* (**Paper II**). Substantially higher contrast thresholds were required in DM images to obtain the same level of detectability as in in-plane BT slices for 1 mm lesions and larger. However, a higher contrast threshold was needed in in-plane BT slices for the 0.2 mm lesion compared with DM images. If twice the dose was used in BT instead, the results suggest that a lower contrast threshold may be needed compared to DM for the detection of the 0.2 mm lesions, although this finding was not statistically significant.

- *The visibility of 3D distributed masses and microcalcification clusters in reconstructed BT image volumes and DM images* (**Paper III**). The visibility of the 8 mm mass was improved with BT image volumes when compared with DM images at both BT dose levels, which indicates that the effect of the superimposed anatomy is substantially reduced with BT. A statistically significant difference was found between the dose levels for the microcalcification clusters, suggesting that detection performance in BT is hampered at the dose level used in DM but is not substantially different when doubling the dose level.

- *Evaluation on how BT image volumes can be read efficiently, using a free-response study combined with eye tracking* (**Paper IV**). Four viewing procedures and two presentation modes in BT image volumes have been evaluated. Although not statistically significantly different in terms of detection performance, the results indicate that viewing BT image volumes horizontally is better when utilizing free scroll browsing only or combined with a cine loop at fast frame rates. The overall impression, was that all tested conditions were promising, except for reading BT image volumes at slow frame rates (i.e. 9 fps).

5 Acknowledgements

First of all, I would like to acknowledge Ingvar Andersson for always being involved in my crazy projects and supporting me. You are my oldest friend, flooded with wisdom and have a great sense of humor! You are the master of breasts! Then I would like to thank my supervisors, Anders Tingberg and Sören Mattsson, for keeping up with me, helping me out in difficult times and being great conference buddies! Longing for more crocodile wings! Magnus Båth, you are the real engine and bass player in my projects, always with new thoughts/inspirations and deep insight! Without you, I would still be in kindergarten! The great author Mark Ruschin, you were my true mentor. Hope to see you again soon! Sune Svensson, the ViewDEXman, thank you for efforts in modifying ViewDEX.

Dev Chakraborty, a true music and JAFROC lover. It has always been an honor to work with you! Thanks for putting in so much effort in my work and I hope to collaborate with you in the future! I would also like to thank Craig Abbey, Ivan Diaz and Thomas Mertelmeier for exchanging great ideas! Thank you to all participating radiologists: Marianne Löfgren, Cecilia Wattsgård, Barbara Ziemiecka and Annika Lindahl.

I would like to thank my friends Sophia Zackrisson and Stina Lång for helping me out in a fun and demanding eye-tracking study. It was a real eye opener! Kenneth Holmqvist, Marcus Nyström, my new fellows in Lund! You are both great eye tracking experts and have inspiried me a lot! Philippe Wagner, a statistician in his own class! Hope to collaborate with all of you!

I would also like to thank my colleagues: Grillmästare Jonas Svensson and Sven Månsson, Reason Mikael Gunnarsson, Herr Wallenius, Bengt Hemdal, Rääfen, and Snickarmästar Sven Brink! Dear PhD friends and coworkers, it has been a pleasure and adventure to work with you: Daniel and Marcus my Aruba darlings, Sillastryparen/vrakletaren/kristallkroneexperten/lumphandlaren Mats Hasson, Pernilla Afrodansare, Calle Altangrillare, Tjernobyl Christian, Hästmotortokiga Marie-Louise, Andreas Weibullfrö, Magnus Hustler, Martin X-jubbare, Marie Sydoff, Fredrik Nordström, Angelica Svalkvist, Sara Asplund, Therese Nilsson, Sofie Ceberg, Hanna Holstein, Therese Geber, Ylva Ranebo, Where is Tony? Svahn, FreDa49, Robban, Pålle, Johan Ö, Johan C and those of you that I have forgot to mention!

Finally, I LOVE YOU: Min Älskling ♡! Mo, Pa, Ka, Chri, and Borgudds!
Groove on Rustybeat, Apeybeat and Jazzmahal!

6 References

Abrams R, Christ S. (2003): Motion onset captures attention. Psychological Science 14(5):427-432.

Andersson I, Ikeda DM, Zackrisson S, Ruschin M, Svahn T, Timberg P, Tingberg A. (2008): Breast tomosynthesis and digital mammography: a comparison of breast cancer visibility and BIRADS classification in a population of cancers with subtle mammographic findings. Eur Radiol 18(12):2817-25.

Anstis SM. (1974): A chart demonstrating variations in acuity with retinal position. Vision Res 14(7):589-92.

Åslund M, Cederström Br, Lundqvist M, Danielsson M. (2007): Physical characterization of a scanning photon counting digital mammography system based on Si-strip detectors. Med Phys 34(6): 1918.

Banks M, Sekuler A, Anderson S. (1991): Peripheral spatial vision: limits imposed by optics, photreceptors, and recepto pooling. J. Opt. Soc. Am. A 8(11):1775-1787.

Båth M, Håkansson M, Tingberg A, Månsson LG. (2005): Method of simulating dose reduction for digital radiographic systems. Radiat Prot Dosim 114(1-3):253-9.

Bissonnette M, Hansroul M, Masson E, Savard S, Cadieux S, Warmoes P, Gravel D, Agopyan J, Polischuk B, Haerer W and others. (2005): Digital breast tomosynthesis using an amorphous selenium flat panel detector. Proc SPIE 5745:529-540.

Bochud FO, Abbey CK, Eckstein MP. (2004): Search for lesions in mammograms: statistical characterization of observer responses. Med Phys 31(1):24-36.

Bochud FO, Valley JF, Verdun FR, Hessler C, Schnyder P. (1999): Estimation of the noisy component of anatomical backgrounds. Med Phys 26(7):1365-70.

Börjesson S, Håkansson M, Båth M, Kheddache S, Svensson S, Tingberg A, Grahn A, Ruschin M, Hemdal B, Mattsson S and others. (2005): A software tool for increased efficiency in observer performance studies in radiology. Radiat Prot Dosim 114(1-3):45-52.

Bunch PC, Hamilton JF, Sanderson GK, AH S. (1978): A free-response approach to the measurement and characterization of radiographic-observer performance. J Appl Photogr Eng 4(4):166-171.

Burgess A, Jacobson F, Judy P. (2003): Mass discrimination in mammography: experiments using hybrid images. Acad Radiol 10 (11):1247-56.

Burgess AE. (1995): Comparison of receiver operating characteristic and forced choice observer performance measurement methods. Med Phys 22(5):643-55.

Burgess AE, Jacobson FL, Judy PF. (2001): Human observer detection experiments with mammograms and power-law noise. Med Phys 28 (4):419-37.

Chakraborty D. (2008): Validation and Statistical Power Comparison of Methods for Analyzing Free-response Observer Performance Studies. Acad Radiol 15(12):1554-1566.

Chakraborty DP. (2010): A status report on free-response analysis. Radiat Prot Dosim 139(1-3):20-5.

Chakraborty DP, Berbaum KS. (2004): Observer studies involving detection and localization: modeling, analysis, and validation. Med Phys 31 (8):2313-30.

Chakraborty DP, Winter LH. (1990): Free-response methodology: alternate analysis and a new observer-performance experiment. Radiology 174(3 Pt 1):873-81.

Chawla A, Saunders R, Abbey CK, Delong D, Samei E. (2006): Analyzing the effect of dose reduction on the detection of mammographic lesions using mathematical observer models. Proc SPIE 6146:61460I.1-61460I.x.

Dance DR, Skinner CL, Young KC, Beckett JR, Kotre CJ. (2000): Additional factors for the estimation of mean glandular breast dose using the UK mammography dosimetry protocol. Phys Med Biol 45 (11):3225-40.

Deubel H. (2008): The time course of presaccadic attention shifts. Psychological Research 72(6):630-640.

Eckstein MP, Abbey CK, Bochud FO. 2000. A practical guide to model observers for visual detection in synthetic and natural noisy images. In: Beutel J, Kundel HL, Van Metter RL, editors. Handbook of Medical Imaging. Volume 1. Physics and Psychophysics. Bellingham: SPIE Press. p 593-628.

Efron B. 1982. The jackknife, the bootstrap, and other resampling plans. Philadelphia, PA: Society for Industrial and applied mathematics.

Efron B, Tibshirani RJ. 1994. An introduction to the Bootstrap: Chapman & Hall/CRC.

Engel F. (1977): Visual conspicuity, visual search and fixation tendencies of the eye. Vision Research 17(1):95-108.

Franconeri SL, Simons DJ. (2003): Moving and looming stimuli capture attention. Percept Psychophys 65(7):999-1010.

Gennaro G, Toledano A, di Maggio C, Baldan E, Bezzon E, La Grassa M, Pescarini L, Polico I, Proietti A, Toffoli A and others. (2010): Digital breast tomosynthesis versus digital mammography: a clinical performance study. Eur Radiol 20(7):1545-53.

Good WF, Abrams GS, Catullo VJ, Chough DM, Ganott MA, Hakim CM, Gur D. (2008): Digital breast tomosynthesis: a pilot observer study. Am J Roentgenol 190(4):865-9.

Gur D, Abrams GS, Chough DM, Ganott MA, Hakim CM, Perrin RL, Rathfon GY, Sumkin JH, Zuley ML, Bandos AI. (2009): Digital breast tomosynthesis: observer performance study. Am J Roentgenol 193(2):586-91.

Håkansson M, Svensson S, Zachrisson S, Svalkvist A, Båth M, Månsson LG. (2010): ViewDEX: an efficient and easy-to-use software for observer performance studies. Radiat Prot Dosim 139(1-3):42-51.

Hemdal B, Andersson I, Grahn A, Håkansson M, Ruschin M, Thilander-Klang A, Båth M, Börjesson S, Medin J, Tingberg A and others. (2005): Can the average glandular dose in routine digital mammography screening be reduced? A pilot study using revised image quality criteria. Radiat Prot Dosim 114(1-3):383-8.

Hemdal B, Bay TH, Bengtson G, Gangeskar L, Martinsen AC, Pedersen K, Thilander Klang A, Mattsson S. Comparison of screen-film, image plate and direct digital mammography with CD phantoms. In: Ed. Peitgen H-O, editor; 2002; Bremen, Germany. Springer verlag Berlin. p 105-107.

Holmqvist K, Nyström N, Andersson R, Dewhurst R, Jarodzka H, van de Weijer J. 2011. Eye tracking: a comprehensive guide to methods and measures. Oxford, UK: Oxford University Press.

Hu YH, Zhao B, Zhao W. (2008): Image artifacts in digital breast tomosynthesis: investigation of the effects of system geometry and reconstruction parameters using a linear system approach. Med Phys 35(12):5242-52.

Huda W, Ogden KM, Scalzetti EM, Dance DR, Bertrand EA. (2006): How do lesion size and random noise affect detection performance in digital mammography? Acad Radiol 13(11):1355-66.

Kundel HL. (1975): Peripheral vision, structured noise and film reader error. Radiology 114:269-273.

Kundel HL, Nodine CF. (1975): Interpreting chest radographs without visual search. Radiology 116:527-532.

Kundel HL, Nodine CF, Conant EF, Weinstein SP. (2007): Holistic component of image perception in mammogram interpretation: gaze-tracking study. Radiology 242(2):396-402.

Kundel HL, Nodine CF, Krupinski EA, Mello-Thoms C. (2008): Using gaze-tracking data and mixture distribution analysis to support a holistic model for the detection of cancers on mammograms. Acad Radiol 15(7):881-6.

Kundel HL, Nodine CF, Toto L. (1991): Searching for lung nodules: the guidance of visual scanning. Invest Radiol 26:777-781.

Laming D, Warren R. (2000): Improving the detection of cancer in the screening of mammograms. J Med Screen 7(1):24-30.

Lauritsch G, Haerer W. (1998): A theoretical framework for filtered backprojection in tomosynthesis. SPIE 3338:1127-1137.

Lefebvre F, Benali H, Gilles R, Di Paola R. (1994): A simulation model of clustered breast microcalcifications. Med Phys 21(12):1865-74.

Litchfield D, Ball LJ, Donovan T, Manning DJ, Crawford T. (2010): Viewing another person's eye movements improves identification of pulmonary nodules in chest x-ray inspection. Journal of experimental psychology. Applied 16(3):251-62.

Mahesh M. (2004): AAPM/RSNA physics tutorial for residents: digital mammography: an overview. Radiographics 24(6):1747-60.

Manning D, Barker-Mill SC, Donovan T, Crawford T. (2006): Time-dependent observer errors in pulmonary nodule detection. Br J Radiol 79(940):342-6.

Manning DJ. (2004): Detection or decision errors? Missed lung cancer from the posteroanterior chest radiograph. Br J Radiol 77(915):231-235.

Megaw E, J. R. (1979): Eye movements and industrial inspection. Applied Ergonomics 10(3):145-154.

Mello-Thoms C. (2006a): How does the perception of a lesion influence visual search strategy in mammogram reading? Acad Radiol 13(3): 275-88.

Mello-Thoms C. (2006b): The problem of image interpretation in mammography: effects of lesion conspicuity on the visual search strategy of radiologists. Br J Radiol 79 Spec No 2:S111-6.

Mello-Thoms C, Hardesty L, Sumkin J, Ganott M, Hakim C, Britton C, Stalder J, Maitz G. (2005): Effects of lesion conspicuity on visual search in mammogram reading. Acad Radiol 12(7):830-40.

Mertelmeier T. Optimizing filtered backprojection reconstruction for a breast tomosynthesis prototype device; 2006. p 6142 61420F-61421-61412.

Metz CE. (1986): ROC methodology in radiologic imaging. Invest Radiol 21(9):720-33.

Metz CE. 2000. Fundamental ROC analysis. In: Beutel J, Kundel HL, Van Metter RL, editors. Handbook of Medical Imaging. Volume 1. Physics and Psychophysics. Bellingham: SPIE Press. p 751-769.

Moraal J. (1975): The analysis of an inspection task in the steel industry. Human Reliability in Quality Control:217-219.

Myers KJ. 2000. Ideal observer models of visual signal detection. In: Beutel J, Kundel HL, Van Metter RL, editors. Handbook of Medical Imaging. Volume 1. Physics and Psychophysics. Bellingham: SPIE Press. p 559-592.

Niklason LT, Christian BT, Niklason LE, Kopans DB, Castleberry DE, Opsahl-Ong BH, Landberg CE, Slanetz PJ, Giardino AA, Moore R and others. (1997): Digital tomosynthesis in breast imaging. Radiology 205(2):399-406.

Nodine CF, Mello-Thoms C, Kundel HL, Weinstein SP. (2002): Time course of perception and decision making during mammographic interpretation. Am J Roentgenol 179(4):917-23.

Noel A, Thibault F. (2004): Digital detectors for mammography: the technical challenges. Eur Radiol 14(11):1990-8.

Ojanpaa HR, Nasanen R, Kojo I. (2002): Eye movements in visual search of word lists. Vision Res 42(12):1499-1512.

Orman J, Mertelmeier T, Haerer W. Adaptation of image quality using various filter setups in the filtered backprojection approach for digital breast tomosynthesis. In: Eds. Astley SM, Brady M, Rose C, Zwiggelaar R, editors; 2006; Manchester, UK. Springer Verlag Berlin. p 175-182.

Philips MH, Edelman JA. (2008): The dependence of visual scanning performance on search direction and difficulty. Vision Res 48(21): 2184-92.

Pisano ED, Gatsonis C, Hendrick E, Yaffe M, Baum JK, Acharyya S, Conant EF, Fajardo LL, Bassett L, D'Orsi C and others. (2005): Diagnostic performance of digital versus film mammography for breast-cancer screening. N Engl J Med 353(17):1773-83.

Pisano ED, Yaffe MJ. (2005): Digital mammography. Radiology 234(2): 353-62.

Poplack SP, Tosteson AN, Grove MR, Wells WA, Carney PA. (2000): Mammography in 53,803 women from the New Hampshire mammography network. Radiology 217(3):832-40.

Reiser I, Nishikawa RM. (2010): Task-based assessment of breast tomosynthesis: effect of acquisition parameters and quantum noise. Med Phys 37(4):1591-600.

Rosenberg RD, Yankaskas BC, Hunt WC, Ballard-Barbash R, Urban N, Ernster VL, Kerlikowske K, Geller B, Carney PA, Taplin S. (2000): Effect of variations in operational definitions on performance estimates for screening mammography. Acad Radiol 7(12):1058-68.

Rowlands JA. 2000. Flat panel detectors for digital radiography. In: Beutel J, Kundel HL, Van Metter RL, editors. Handbook of Medical Imaging. Volume 1. Physics and Psychophysics. Bellingham: SPIE Press. p 223-328.

Rowlands JA. (2002): The physics of computed radiography. Phys Med Biol 47(23):R123-66.

Ruschin M, Tingberg A, Båth M, Grahn A, Håkansson M, Hemdal B, Andersson I. (2005): Using simple mathematical functions to simulate pathological structures--input for digital mammography clinical trial. Radiat Prot Dosim 114(1-3):424-31.

Saunders R, Samei E. (2004): Characterization of breast masses for simulation purposes. Proc SPIE 5372:242-250.

Saunders R, Samei E, Baker J, Delong D. (2006): Simulation of mammographic lesions. Acad Radiol 13(7):860-70.

Skaane P. (2009): Studies Comparing Screen-Film Mammography and Full-Field Digital Mammography in Breast Cancer Screening: Updated Review. Acta Radiol 50(1):3-14.

Svalkvist A, Båth M. (2010): Simulation of dose reduction in tomosynthesis. Med Phys 37(1):258.

Svane G, Azavedo E, Lindman K, Urech M, Nilsson J, Weber N, Lindqvist L, Ullberg C. (2011): Clinical experience of photon counting breast tomosynthesis: comparison with traditional mammography. Acta radiol 52(2):134-42.

Teertstra HJ, Loo CE, van den Bosch MA, van Tinteren H, Rutgers EJ, Muller SH, Gilhuijs KG. (2010): Breast tomosynthesis in clinical practice: initial results. Eur Radiol 20(1):16-24.

Timberg P, Ruschin M, Båth M, Hemdal B, Andersson I, Mattsson S, Chakraborty D, Saunders R, Samei E, Tingberg A. (2006): Potential for lower absorbed dose in digital mammography: A JAFROC experiment using clinical hybrid images with simulated dose reduction. Proc SPIE 6146:341-350.

Tingberg A, Förnvik D, Mattsson S, Svahn T, Timberg P, Zackrisson S. (2011): Breast Cancer Screening with Tomosynthesis--Initial Experiences. Radiat Prot Dosim.

Wu T, Moore RH, Rafferty EA, Kopans DB. (2004): A comparison of reconstruction algorithms for breast tomosynthesis. Med Phys 31 (9):2636.

Zhao B, Zhou J, Hu YH, Mertelmeier T, Ludwig J, Zhao W. (2009): Experimental validation of a three-dimensional linear system model for breast tomosynthesis. Med Phys 36(1):240-51.

Zoetelief J, Fitzgerald M, Leitz W, Säbel M. (1996): European protocol on dosimetry in mammography. EUR 16263